RMS EMITTANCE MEASURES FOR SOLENOID TRANSPORT AND FACILITY FOR RARE ISOTOPE BEAMS FRONT-END SIMULATIONS*

Steven M Lund†, Eduard Pozdeyev, Haitao Ren, and Qiang Zhao
Facility for Rare Isotope Beams, Michigan State University, East Lansing, MI , USA 48824

Abstract

Measurement of beam phase-space area via rms emittances in solenoid focusing channels with x-y coupling is complicated relative to transport channels with decoupled plane focusing. This stems from correlated azimuthal flow of the beam induced by the coupled focusing influencing how the thermal component of the flow should be measured. This is exacerbated when the beam has net canonical angular momentum — as is the case for beams born in a magnetic field within ECR-type sources. In this study, a systematic analysis is carried out to derive an multi-species beam envelope equation and motivate measures of rms emittance and phase-space area for use in solenoid transport for beams with canonical angular momentum. These results are applied in Warp PIC simulations of the near-source region of the front-end of the Facility for Rare Isotope Beams (FRIB) linac. In these simulations, a multi-species heavy-ion DC beam emerging from an ECR source are simulated in transverse slice mode using a realistic lattice description. Emittance growth due to nonlinear applied fields and space-charge is analyzed including the influence of net canonical angular momentum. It is found that emittance growth in the near source region of FRIB front-end should in most cases be minimal and that the beam size can be readily controlled over a wide range of parameter uncertainties.

INTRODUCTION

The Facility for Rare Isotope Beams (FRIB) is a high continuous-wave power (CW) linear accelerator now under construction at Michigan State University to enable state-of-the-art nuclear physics experiments [1]. It will simultaneously accelerate multiple charge states of heavy ions to kinetic energies above 200 MeV/u with 400 kW power on target delivered within a compact spot. Although the FRIB linac has high CW power, space-charge intensity is modest in most of the machine. However, near the electron cyclotron resonance (ECR) sources in the front end (see Fig. 1), space-charge can be an issue [2]. Here, kinetic energy is low (~ 35 kV ECR extraction bias followed by a grated dc gap typically biased to ~ 50 kV to achieve 12 kV/u in target species) and the ECRs produce numerous charge states and ions resulting in relatively high DC current until extra species are removed downstream beginning with the first bending dipole. Uranium and Oxygen species, (unneutralized) particle currents, and particle rigidities (at extractor bias) expected for Uranium ECR operation are given in Table 1. It is anticipated that space-charge of the DC beam will be ~ 75% electron neutralized outside of the grated gap (strong sweep and guarded downstream by a negatively biased suppressor electrode). Typically only two target species will be transported downstream of the front-end. A compact beam phase-space (low emittance and halo suppressed) in the target species must be preserved in transport near the source in the presence of the parasitic species to insure reliable machine operation with minimal potential losses. In the transport immediately downstream of the ECR two solenoids are employed to transversely focus the multi-species beam. Solenoids are short with poor aspect ratio (39.5 cm length and 7.75 cm radius aperture) and the extended fringe fields overlap with the solenoid field from the ECR source and the grated gap. Ions are born relatively cold (expect ~ 1–3 eV thermal temperature expected) with a compact radius ($R \simeq 4$ mm) but are strongly magnetized in the hight magnetic fields within the ECR sources resulting in significant canonical angular momentum contributions to the transverse beam size.

Table 1: (Color) Species from FRIB Venus-like ECR source for U operation. Color coding shown for species identification in simulations. U^{+33} and U^{+34} are target species.

Ion	I (pmA)	Q/A	$[B\rho]$ (Telsa-m)
U^{+25}	0.035	0.105	0.0831
U^{+26}	0.051	0.109	0.0815
U^{+27}	0.068	0.113	0.0800
U^{+28}	0.088	0.118	0.0785
U^{+29}	0.115	0.122	0.0772
U^{+30}	0.150	0.126	0.0759
U^{+31}	0.175	0.130	0.0746
U^{+32}	0.192	0.134	0.0735
U^{+33}	0.210	0.139	0.0723
U^{+34}	0.205	0.143	0.0713
U^{+35}	0.178	0.147	0.0702
U^{+36}	0.142	0.151	0.0693
U^{+37}	0.11	0.155	0.0683
U^{+38}	0.072	0.160	0.0674
U^{+39}	0.043	0.163	0.0665
U^{+40}	0.031	0.168	0.0657
O^{+1}	0.3	0.063	0.1077
O^{+2}	0.3	0.125	0.0762
O^{+3}	0.3	0.188	0.0622
O^{+4}	0.2	0.250	0.0539

In this study we employ theory to develop an envelope model (Sec. Envelope Model) and report preliminary particle-in-cell simulations with the Warp code [3] (Sec. Simulations). The envelope model is employed to better understand how to measure effective beam phase-space area for the multi-species beam with canonical angular momentum and solenoid focusing which both induce coherent azimuthal flow in the beam components. The simulations

* Work supported by the U.S. Department of Energy Office of Science under Cooperative Agreement DE-SC0000661 and the National Science Foundation under Grant No. PHY-1102511.
† lund@frib.msu.edu

ISBN 978-3-95450-173-1

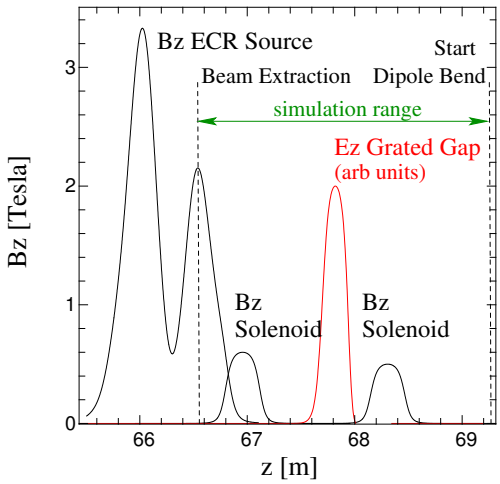

Figure 1: (Color) Applied fields (on-axis nonlinear components) of FRIB front-end near ECR source. FRIB lattice reference $z = 200$ m at the start of the RFQ.

allow inclusion of detailed geometry, multiple species with part electron neutralization, and coupled dynamics with solenoid focusing and overlapping element fringe fields. The simulations enable evaluation of system performance under increasingly realistic conditions.

ENVELOPE MODEL

A systematic derivation of an rms envelope equation describing an unbunched, multi-species DC beam propagating in a solenoid focusing channel with electrostatic accelerating gaps is carried out to better understand how to measure the effective phase-space area (emittance) and the relative strength of various focusing/defocusing effects. Consider a species j composed of particles of mass m_j and charge q_j propagating with axial velocity $\beta_{bj}c$ with c the speed of light in *vacuuo*. The nonrelativistic transverse equations of motion describing the particles evolving in a applied solenoid magnetic field (linear approximation) $\mathbf{B}^{\rm appl} = -\frac{1}{2}\frac{\partial B_{z0}(z)}{\partial z} r\hat{\mathbf{e}}_r + B_{z0}(z)\hat{\mathbf{e}}_z$ with $B_{z0}(z) = B_z(r = 0, z)$ the on-axis magnetic field and an applied electric accelerating field from electrostatic gaps (linear approximation) $\mathbf{E}^{\rm appl} = -\frac{1}{2}\frac{\partial E_{z0}(z)}{\partial z} r\hat{\mathbf{e}}_r + E_{z0}(z)\hat{\mathbf{e}}_z$ with on-axis field $E_{z0}(z) \equiv E_z^a(r = 0, z)$ can be cast in the form [4, 5]

$$\begin{aligned} &x'' - \frac{q_j V'}{2\mathcal{E}_{kj}}x' - \frac{q_j V''}{4\mathcal{E}_{kj}}x - \frac{q_j B'_{z0}}{2m_j\beta_{bj}c}y - \frac{q_j B_{z0}}{m_j\beta_{bj}c}y' \\ &\quad = \frac{q_j}{m_j\beta_{bj}^2 c^2}E_x^{self}, \\ &y'' - \frac{q_j V'}{2\mathcal{E}_{kj}}y' - \frac{q_j V''}{4\mathcal{E}_{kj}}y + \frac{q_j B'_{z0}}{2m_j\beta_{bj}c}x + \frac{q_j B_{z0}}{m_j\beta_{bj}c}x' \\ &\quad = \frac{q_j}{m_j\beta_{bj}^2 c^2}E_y^{self}. \end{aligned} \tag{1}$$

Here, primes denote derivatives with respect to the axial coordinate z, $E_x^{\rm self}$ and $E_x^{\rm self}$ are the transverse components of the electrostatic self-electric field of the beam, and $V(z)$ is the accelerating potential that relates to the on-axis applied electric field via $E_{z0}(z) = -\frac{\partial V(z)}{\partial z}$ and gives the gain in particle axial velocity $\beta_{bj}c$ and kinetic energy $\mathcal{E}_{kj} = \frac{1}{2}m_j\beta_{bj}^2 c^2$ from the initial value as

$$\begin{aligned} \mathcal{E}_{kj} &= \mathcal{E}_{kj}|_{\rm initial} + q_j[V|_{\rm initial} - V], \\ \beta_{bj} &= \sqrt{\frac{2\mathcal{E}_{kj}}{m_j c^2}}. \end{aligned} \tag{2}$$

Note that the x- and y-plane particle equations of motion 1 are cross-coupled due to the solenoid focusing field. Both the applied magnetic (solenoid focusing) and electric (accelerating) fields include fringe effects from the axial variation in z which produces consistent focusing/defocusing effects within the approximation of linear applied fields.

To derive an envelope equation, we neglect energy spreads within each species and carry out transverse averages $\langle\cdots\rangle_j$ over the jth species and analyze the rms radius $\sigma_{rj} \equiv \langle x^2 + y^2\rangle_j^{1/2}$. As standard, σ_{rj} is differentiated several times with respect to z and the equations of motion (1) are applied to calculate $\langle xx''\rangle_j$ and $\langle yy''\rangle_j$ [4]. An extensive analysis with the additional assumption that the charge distributions of the species are axisymmetric ($\partial/\partial\theta = 0$) with Gaussian distributed radial density profiles (possibly part electron neutralized) shows that the rms envelope equation for the jth species can be expressed as

$$\begin{aligned} &\sigma''_{rj} - \frac{q_j V'}{2\mathcal{E}_{kj}}\sigma'_{rj} - \frac{q_j V''}{4\mathcal{E}_{kj}}\sigma_{rj} + \left(\frac{q_j B_{z0}}{2m_j\beta_{bj}c}\right)^2\sigma_{rj}, \\ &\quad - \sum_{s,\,\rm species} Q_{js} f_s \frac{\sigma_{rj}}{\sigma_{rj}^2 + \sigma_{rs}^2} \\ &\quad - \frac{\varepsilon_{rj}^{\rm rms\ 2} + \langle P_\theta\rangle_j^2/(m_j\beta_{bj}c)^2}{\sigma_{rj}^3} = 0. \end{aligned} \tag{3}$$

Here,

$$Q_{js} = \frac{q_j I_s}{2\pi\epsilon_0 m_j\beta_{bj}^2\beta_{bs}c^3} \tag{4}$$

is the "matrix" preveance that measures the strength of species s space-charge associated with current $I_s = $ const (electron neutralized by specified fraction $f_s \in [0, 1]$ with $f_s = 1$ being unneutralized) of species s on the jth species, ϵ_0 is the permitivity of free-space,

$$\begin{aligned} \frac{\langle P_\theta\rangle_j}{m_j\beta_{bj}c} &= \langle xy' - yx'\rangle_j + \frac{q_j B_{z0}}{2m_j\beta_{bj}c}\langle x^2 + y^2\rangle_j \\ &= \langle r^2\theta'\rangle_j + \frac{qB_{z0}}{2m\beta_b c}\langle r^2\rangle_j \end{aligned} \tag{5}$$

specifies the average canonical angular momentum $\langle P_\theta\rangle_j$ of species j, and

$$\begin{aligned} \varepsilon_{rj}^{\rm rms\ 2} &= \langle x^2 + y^2\rangle_j\langle x'^2 + y'^2\rangle_j - \langle xx' + yy'\rangle_j^2 \\ &\quad - \langle xy' - yx'\rangle_j^2 \\ &= \langle r^2\rangle_j\langle r'^2\rangle_j - \langle rr'\rangle_j^2 + \langle r^2\theta'^2\rangle_j - \langle r^2\theta'\rangle_j^2 \end{aligned} \tag{6}$$

ISBN 978-3-95450-173-1

is a proper *thermal* (i.e., coherent flow contribution induced by solenoid removed) measure of the transverse phase-space area. Both $\langle P_\theta \rangle_j$ and $\varepsilon_{rj}^{\rm rms}$ are given in both transverse x,y Cartesian components and r,θ cylindrical coordinates. The canonical angular momentum $\langle P_\theta \rangle_j$ is conserved (even for nonlinear self-field forces), and for the case of linear or negligible self-field forces, it can be shown that the normalized thermal emittance

$$\varepsilon_{nrj}^{\rm rms} \equiv \beta_{bj}\varepsilon_{rj}^{\rm rms} = \text{const} \tag{7}$$

is also conserved. Note that the applied focusing coefficient from the solenoid focusing in Eq. (3) can be expressed as $[q_j B_{z0}/(2m_j\beta_{bj}c)]^2\sigma_{rj} = k_{Lj}^2\sigma_{rj}$ where $k_{Lj} \equiv q_j B_{z0}/(2m_j\beta_{bj}c)$ is the Larmor wavenumber. Employing the conservations in Eqs. (5) and (7) allows integration of the envelope equation (3) from a specified initial condition.

It should be stressed that all terms occurring in Eq. (3) are *independent* of the details of the transverse distribution (and are therefore valid for nonaxisymmetric species with $\partial/\partial\theta \neq 0$) with exception of the space-charge (perveance) term $\propto Q_{js}$ which requires axisymmetry for the relatively simple form given. Inter-species coupling is provided only by the radial electrostatic force acting on the particles which the space-charge term describes. The perveance term is derived by taking the species radial charge density profile to have Gaussian form with

$$\rho_j(r) = \frac{I_j}{2\pi\beta_{bj}c\,\sigma_{rj}^2} e^{-r^2/\sigma_{rj}^2}, \tag{8}$$

and solving the electrostatic Gauss' law Maxwell equation $\frac{1}{r}\frac{\partial}{\partial r}(rE_r^{\rm self}) = \sum_{\rm species,\,s}\frac{f_s\rho_s}{\epsilon_0}$ (axial self-fields neglected) for the radial self-electric field as

$$E_r^{\rm self} = \sum_{s,\rm species}\frac{f_s}{2\pi\epsilon_0}\frac{\lambda_s(r)}{r}, \tag{9}$$

where $\lambda_s(r) = 2\pi\int_0^r d\bar{r}\,\bar{r}\rho_s(\bar{r})$ is the line-charge of species s within radius r [$\lambda_s(\infty) = I/(\beta_b s)$]. Using this result, the average $\langle rE_r^{\rm self}\rangle_j$ needed to derive the perveance term in Eq. (3) can be calculated using the result

$$\langle\lambda_s(r)\rangle_j = \left(\frac{I_s}{\beta_{bs}c}\right)\frac{\sigma_{rj}^2}{\sigma_{rj}^2+\sigma_{sj}^2} \tag{10}$$

to express contributing terms. Interestingly, it can be shown that the $s = j$ component of the perveance term in Eq. (3) is independent of the form of the radial charge distribution — suggesting somewhat broader validity of the envelope equation than just Gaussian distributed radial charge profiles [4, 6]. If there is a single species, the perveance term reduces (independent of the form of the radial charge distribution) to the familiar form $Qf/(2\sigma_r)$ with $Q = \frac{qI}{2\pi\epsilon_0 m\beta_b^3 c^3}$. Here, we drop the species subscripts since there is one species. Comparing the perveance (space-charge defocusing strength) and the emittance + canonical angular momentum (phase-space area defocusing) terms in the envelope equation (3), note that the space-charge term will eventually dominate as the beam radially expands (term $\sim 1/\sigma_{rj}$), and conversely, the emittance + canonical angular momentum term eventually dominates as the beam is radially focused down ($\sim 1/\sigma_{rj}^3$).

The envelope equation (3) shows that the total effective phase-space area acting to defocus beam species j is

$$\varepsilon_{{\rm tot}j}^{\rm rms} \equiv \sqrt{\varepsilon_{rj}^{\rm rms\,2} + \frac{\langle P_\theta\rangle_j^2}{(m_j\beta_{bj}c)^2}}. \tag{11}$$

The total emittance $\varepsilon_{{\rm tot}j}^{\rm rms}$ contains a component $\varepsilon_{rj}^{\rm rms}$ [Eq. (6)] from the thermal spread of particle angles (normalized form $\beta_{bj}\varepsilon_{rj}^{\rm rms}$ conserved for linear forces) and component $\langle P_\theta\rangle_j^2$ [Eq. (5)] from the coherent flow associated with canonical angular momentum (conserved nonlinearly if a consistent nonlinear form for the associated magnetic vector potential is employed). Properties of the thermal emittance can be further clarified by the axisymmetric ($\partial/\partial\theta = 0$) limit formula,

$$\varepsilon_{rj}^{\rm rms\,2} = 4\varepsilon_{xj}^{\rm rms\,2} - \langle xy' - yx'\rangle_j^2 \tag{12}$$

with $\varepsilon_{xj}^{\rm rms} \equiv \left[\langle x^2\rangle_j\langle x'^2\rangle_j - \langle xx'\rangle_j^2\right]^{1/2}$ denoting the usual x-plane rms emittance. This clarifies within the simpler axisymmetric limit how the radial emittance $\varepsilon_{rj}^{\rm rms}$ subtracts the coherent flow associated with mechanical angular momentum $\propto \langle xy' - yx'\rangle_j$ to provide a proper thermal measure of the contribution of the spread in particle angles to the emittance. Because the regular x-plane rms emittance $\varepsilon_x^{\rm rms}$ contains (typically large) coherent flow associated with coherent rotation inducted by the solenoid, it provides a poor measure to employ to measure potential emittance growth due to nonlinear applied focusing and space-charge effects. This issue is exacerbated for the case with beams with net canonical angular momentum ($\langle P_\theta\rangle_j \neq 0$) as should be expected for beams produced by ECR type sources. This follows because beams with $\langle P_\theta\rangle_j \neq 0$ will have correlated flow terms in $\varepsilon_x^{\rm rms}$ even outside the axial extent of the fringe field of the magnetic solenoids. Use of the canonical angular momentum $\langle P_\theta\rangle_j^2$ [Eq. (5)], radial thermal emittance $\varepsilon_{rj}^{\rm rms}$ [Eq. (5)], and the total emittance $\varepsilon_{{\rm tot}j}^{\rm rms}$ [Eq. (11)] helps clarify issues in such systems.

For purposes of estimating the emittance of a beam emerging from a source where ions are not born in a state of macroscopic rotation in a finite axial magnetic field ($B_{z0} \neq 0$), Eqs. (5) and (6) suggest taking

$$\begin{aligned}\frac{\langle P_\theta\rangle_j}{m_j c} &= \frac{q_j B_{z0}}{2m_j c}\sigma_{rj}^2\Big|_{\rm Birth}\\ \varepsilon_{nrj}^{\rm rms} = \beta_{bj}\varepsilon_{rj}^{\rm rms} &= \sqrt{2}\sqrt{\left(\frac{T_j}{m_j c^2}\right)}\sigma_{rj}\Big|_{\rm Birth}\end{aligned} \tag{13}$$

Here, T_j is the thermal temperature of the jth ion species (energy units) and the formulas are presented in appropriate form for direct comparison in "normalized" emittance

ISBN 978-3-95450-173-1

units. Both these results neglect the influence of the sextupole field and other physics in the ECR source, and therefore can only be regarded as an estimate of possible characteristic values for such sources.

Finally, we stress that the forms of the canonical angular momentum [Eq. (5)] and radial thermal emittance [Eq. (6)] apply to beams that are not axisymmetric ($\partial/\partial\theta \neq 0$) and can therefore be applied in this generalized context in detailed simulations even if the space-charge term cannot. If there is centroid offset, all terms other than the space-charge perveance one ($\propto Q_{js}$) in the envelope equation (3) also remain valid and can be defined with respect to coordinates relative to the centroid ($x \to x - \langle x\rangle_j$, $x' \to x' - \langle x'\rangle_j$, etc.). These features make the x,y, x',y', versions of the formulas useful for interpreting simulations under increasingly realistic conditions. For an nonaxisymmetric and/or centroid offset beam, the space-charge term becomes considerably more complicated and simulations become more essential.

SIMULATIONS

We employ the Warp particle-in-cell (PIC) code [3] to simulate the transport of the beam emerging from the ECR source to the start of the bending dipole (see Sec. Introduction). The code is run in a transverse (xy) slice mode using the 3D applied fields of elements (axisymmetric solenoids and grated acceleration gap input on a r–z for the aligned system). High resolution models ($\sim$ 1 mm mesh increments in r, z) are employed for the ECR solenoid, focusing solenoids, and the grated gap. Solenoid fringe fields are resolved to $\sim 10^{-6}$ of the peak value and the nonlinear vector potential is input to verify nonlinear conservation of canonical angular momentum. Fringe resolutions of $\sim 10^{-2}$ were found to induce large errors in $\langle P_\theta\rangle_j$. Element fields are input both in linear (using nonlinear on-axis field and the model in Sec. Envelope Model) and nonlinear form to allow nonlinear applied fields to be turned off. Self-fields are calculated with a specified neutralization fraction using a multi-grid field solver ($\lesssim$ 0.5 mm mesh increments in x, y) and any lost particles scraped at the local aperture radius. Macro-particles (typically using > 100 per grid cell within beam corresponding to $\sim$ 40k/species) are advanced in time with individual time increments iterated so that the code tracks from axial slice to axial slice with increment $\Delta z \lesssim 2$ mm. Species weights (physical particles per macro-particle) are adjusted consistent with acceleration from the applied gap DC current conservation in each species to model a slice of the unbunched DC beam. Note this model does not assume beam axisymmetry allowing distribution asymmetries emerging from the ECR and misaligned elements to be evaluated. The xy-slice model neglects any longitudinal self-field effects which should be weak and idealizes electron effects. However, Warp can be run in a 3D mode (inputs/setup essentially the same) to address these issues. The efficient slice model allows rapid (~minutes on PC) simulations to efficiently explore issues.

Simulations are carried out for a Uranium beam injecting the species in Table 1. It is verified that currents and canonical angular momentum are consistent, and that energy gains in the on-axis potential of the gap are correct (gap biased 50.26 kV so average of "target" U^{+33} and U^{+34} species achieves 12 Ks/u). Diagnostics are carried out by species results colorized consistent with entries in Table 1. Emittance measures developed in Sec. Envelope Model are employed to allow sensitive evaluation of emittance evolution in the transport. Series of runs were carried out to explore sensitivities of the target species rms beam envelopes and emittance growth to: unmagnetized (unrealistic: $\langle P_\theta\rangle_j = 0$) and magnetized (estimate appropriate for ECR with $B_{z0} = 2.15$ Tesla giving $\langle P_\theta\rangle_j/(m_j c) \sim$ 0.38 mm-mrad for ref species)initial ions emerging from the ECR source with low ($T_j = 3$ eV giving for all U species $\varepsilon^{\rm rms}_{nrj} = 0.015$ mm-mrad) and high ($T_j = 140$ eV giving for all U species $\varepsilon^{\rm rms}_{nrj} = 0.1$ mm-mrad) ion thermal temperatures, the phase-space form of the initial distribution (thermal and waterbag including self-field potential in the Hamiltonian, semi-Gaussian with uniform density and Gaussian angle spreads, and KV), linear and nonlinear applied fields (both solenoids and grated gap), and electron neutralization fraction (unneutralized, 25%, 50%, 75%, and fully neutralized). In all cases, the same initial axisymmetric beam sizes ($\sigma_{rj}/\sqrt{2} = \langle x^2\rangle_j^{1/2} = \langle y^2\rangle_j^{1/2} = 2.0$ mm and zero angle) were used emerging from the ECR source. Note that the high ion temperature case (i.e., $T_j = 140$ eV) is tuned such that the initial thermal emittance corresponds to measured values (including coherent flow) of the total on a similar ECR source emittance [2,7]. Relatively modest sensitivities were observed in most cases outside of extreme values and the two focusing solenoids are easily adjusted to produce a final (entering dipole) rms beam size $\langle x^2\rangle_j^{1/2} \simeq 10$ mm with a slightly converging envelope (few mrad) for the target species. A partial exception to this is the case of low initial ion temperatures where some normalized thermal emittance ($\varepsilon^{\rm rms}_{nrj}$) growth occurs from very low initial values. But the growth is not sufficient to result in high final emittance or to significantly impact the envelope because the canonical angular momentum contribution to the defocusing [see Eq. (11)] is larger (and constant).

Characteristic results of simulations are shown in Figs. 2 (rms envelope and emittance evolution) and 3 (final phase-space projections of species) for an initial waterbag distribution beam for initially magnetized ions with low temperature, a 75% neutralization fraction, and nonlinear applied fields (solenoids and grated gap). First and second solenoid excitations (see Fig. 1) correspond to 0.6 and 0.5 Tesla peak field on-axis (ECR solenoids fixed for source performance). Cases with the higher initial ion temperature undergo no significant growth. The modest growth for cold initial, but magnetized ions does little to change the effective emittance ($\varepsilon^{\rm rms}_{{\rm tot}j}$) or envelope for initially magnetized ions since the contribution of the canonical angular momentum ($\langle P_\theta\rangle_j$) dominates relative to the contribution from the thermal component of the emittance ($\varepsilon^{\rm rms}_{rj}$) [i.e, see Eq. (11),

ISBN 978-3-95450-173-1

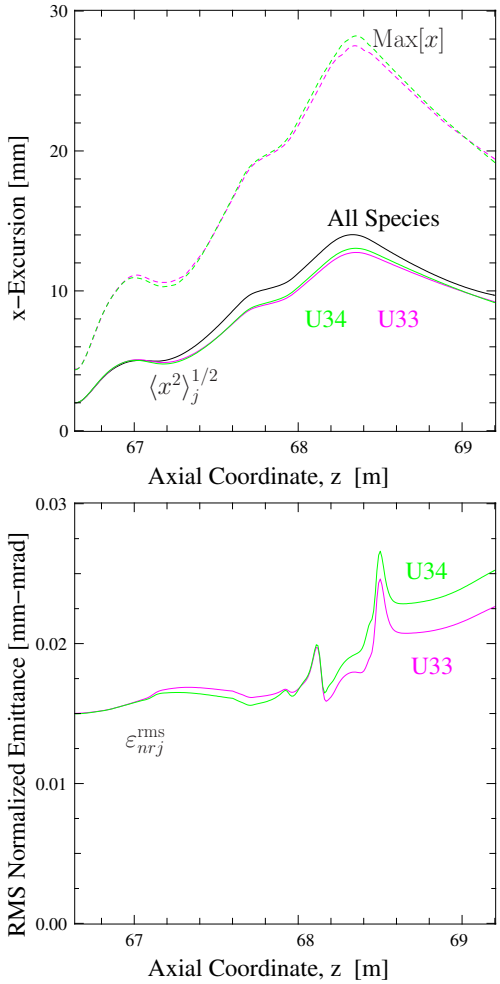

Figure 2: (Color) rms envelope and emittance evolution.

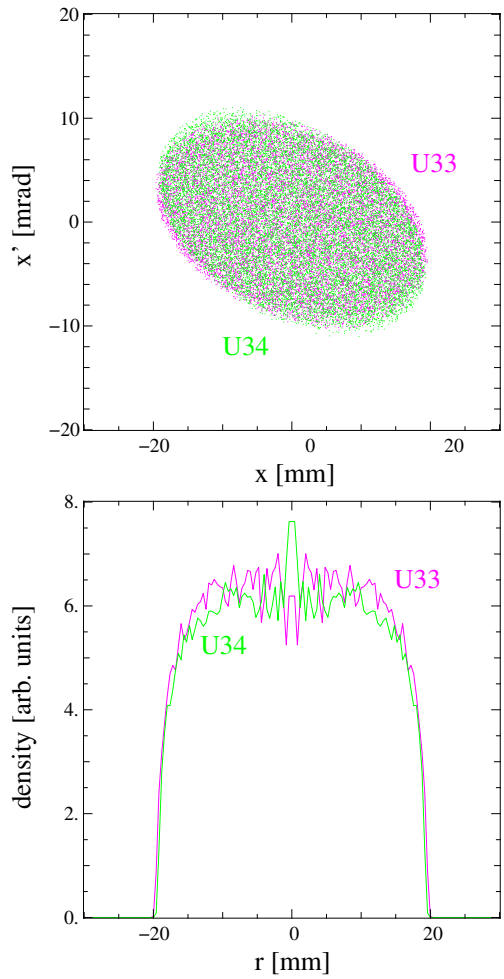

Figure 3: (Color) Phase-space projections at end of simulation (before dipole): particle x-x' with tilt removed, and final target species densities.

$\beta_{bj}\varepsilon^{\rm rms}_{{\rm tot}j} \simeq \langle P_\theta\rangle_j/(m_j c) = 0.38$ mm-mrad]. Phase-space projections of target species (see Fig. 3)) typically have surprisingly low distortion.

CONCLUSIONS

Preliminary theory and simulations of the near-source transport of the FRIB front-end suggests that potential deleterious effects from nonlinear space-charge in the many-species, part electron neutralized beam immediately downstream of the ECR sources (before species separation) is minimal. The system appears relatively insensitive to neutralization fraction and can be retuned for a wide range of potential beam parameters emerging from the sources. Proper separation of coherent flow induced by solenoid focusing and canonical angular momentum in emittance measures allows sensitive probing of contributions to any growth in beam phase-space area. Detailed Warp simulations should help us address any problems encountered during front-end commissioning by augmenting limited laboratory diagnostics. In future work, simulations will be extended downstream to evaluate species separation in the presence of beam space-charge and canonical angular momentum and evaluate the impact of more realistic distributions (including sextupole effects, asymmetries, and halo) to model the beam emerging from the ECR source.

ACKNOWLEDGMENT

The authors benefited from unpublished work by J.J. Barnard (LLNL) on aspects of the envelope model and D.P. Grote (LLNL) provided support for the Warp code.

REFERENCES

[1] J. Wei, et al., LINAC 2012, Tel Aviv, Israel, TU1A04.

[2] E. Pozdeyev, et al., NA-PAC 2013, Pasadena CA, WEOAB1.

[3] For info on the Warp code see: `http://warp.lbl.gov`

[4] S. Lund and J. Barnard, US Particle Accel. School, *Beam Physics with Intense Space Charge,* 2015, 2011: `https://people.nscl.msu.edu/~lund/uspas/bpisc_2015/`

[5] M. Reiser, *Theory and Design of Charged Particle Beams*, (New York: Wiley, 2nd Edition, 2008).

[6] F.J. Sacherer, IEEE Tans. Nuc. Sci. **18**, 1105 (1971).

[7] L. Su, et al., Rev. Sci. Instr. **83**, 02B705 (2012).

ISBN 978-3-95450-173-1